Response of heat release to equivalence ratio variations in high Karlovitz premixed H_2/air flames at 20 atm

Xujiang Wang[a], Tai Jin[a,b*], Kai H. Luo[a*]

[a] Department of Mechanical Engineering, University College London, London WC1E 7JE, UK

[b] State Key Laboratory of Clean Energy Utilization, Zhejiang University, Hangzhou 310027, China

*Corresponding author:

Kai H. Luo

Email: k.luo@ucl.ac.uk

Tai Jin

Email: tai.jin@ucl.ac.uk

Submitted to

International Journal of Hydrogen Energy

Nomenclature

β_i Temperature exponent of Arrhenius equation

δ_L Laminar flame thickness

δ_f Reaction layer thickness

Δx Grid resolution

κ Mean curvature

v Kinematic viscosity

ν'_{kj} Forward stoichiometric coefficient for species k in reaction j

ν''_{kj} Reverse stoichiometric coefficient for species k in reaction j

φ Equivalence ratio of the fresh mixture

φ_L Local equivalence ratio

$\dot{\omega}$ Species reaction rate

A_i Pre-exponential factor of Arrhenius equation

c Progress variable

E_i Activation energy of a reaction

Ka Karlovitz number

K_f Forward reaction rate constant

K_r Reverse reaction rate constant

K_0 Limit of low-pressure reaction rate constant

K_∞ Limit of high-pressure reaction rate constant

K_{ci} Equilibrium constant

l_t Integral length scale

$[M]$ Overall contribution of different species in Three-body reactions

Re Reynolds number

S_L Laminar flame speed

S_{yz} Cross-section area

T Local temperature

T_u Temperature of unburnt gas

T_b Temperature of burnt gas

u' Root-mean-square turbulent velocity fluctuation

V_{rec} Reaction zone volume

X_k Molar concentration of species k

$Y_{f,k}$ Local mass fraction of species k

$Y_{u,k}$ Mass fraction of species k in the fresh mixture

$Y_{b,k}$ Mass fraction of species k in the burnt mixture

Abstract

This paper presents three-dimensional direct numerical simulations of lean premixed H_2/air flames with equivalence ratio 0.4, 0.5 and 0.6, respectively. The initial Karlovitz number is around 2335 and the pressure is 20 atm, which is relevant to gas turbine conditions. The heat release in reaction zones under different equivalence ratios is examined statistically with the aim to extending our understanding of lean combustion under high-pressure conditions. With increasing equivalence ratio, the relative thickness of reaction zone (δ_f/δ_L) is increasing for both laminar and turbulent flames, but the extent of increase is reduced under high equivalence ratio. By examining the local structures of flame fronts, it is found that trenches and plateaus of local equivalence ratio are located on separate sides of the reaction zone edge. Due to the decreased Lewis number under high equivalence ratio, the trench 'depth' and plateau 'height' are reduced. For the flame under ultra-lean conditions, there are some spots with temperatures above adiabatic temperature. This is attributed to the high-fraction of radicals in these regions, which will promote heat release. Furthermore, the heat release rates of elementary reactions are investigated with the analysis of radical fractions and rate constants. When the mixture equivalence ratio varies, the local heat release is changed in different temperature windows due to the combined effects of radical fractions and reaction rate constants.

*Keywords***:** Direct numerical simulation; Lean premixed flame; Heat release rate; Equivalence ratio

1. Introduction

With growing concern about global climate change and increasingly stringent regulations on pollutant emissions, lean premixed combustion has had wide-ranging applications in industrial devices, e.g. stationary gas turbines [1]. In lean premixed combustion, the peak combustion temperature is reduced, leading to lower NO_x emission. However, turbulent lean premixed flames are susceptible to equivalence ratio oscillation, which is one of the most significant mechanisms contributing to combustion instabilities, and local extinction can occur due to variations of equivalence ratio in combustion chambers [2-4]. In modern gas turbines, typical equivalence ratios at base load are in the range of 0.45-0.6 [2]. The turbulent flames in gas turbines are also characterised by intense turbulence intensity and high pressure [5, 6]. The turbulent velocity fluctuation is as high as 150 times of the laminar flame speed and the pressure can reach up to 30 bar in gas turbines [5-7]. Under these critical conditions, flame structures and chemical activities will be dramatically modified [8], and the enhanced turbulence-flame interaction dramatically increases difficulties in experimental and numerical studies. Therefore, it is vital to have a good understanding of fundamental characteristics of lean premixed combustion under conditions relevant to industrial combustion devices, which will promote combustion device developments and combustion model validations.

One crucial unsolved issue in combustion instability is the heat release rate variation with the equivalence ratio, despite numerous experimental and numerical studies [9]. In such a context, a non-dimensional parameter, the Karlovitz number (Ka) [10], was introduced to describe the time scales of flame-turbulence interactions. Under conditions relevant to gas turbines, the Karlovitz number tends to increase to a high level, and turbulent flames will move from the thin reaction zone ($1 < Ka < 100$) towards the distributed reaction zone ($Ka > 100$). It is demonstrated by Stopper et al. [11] that the Karlovitz number is in the range of 77-230 in a swirl burner for industrial gas turbines. Zhou et al. [12] experimentally studied high Ka jet flames with equivalence ratio (φ) 0.4 and 0.7. They found that, under high Ka, rapid transport can significantly change the distribution of radicals and heat release is enhanced in low-temperature regions. Under leaner conditions, it is easier for the flames to

become distributed. Skiba et al. [13] measured the Bunsen-type flame structures in 16 cases with φ = 0.65 and 0.85. They found that the preheat zone is dramatically broadened at high Ka, especially at higher equivalence ratio. However, the thickness of the reaction layer is insensitive to turbulence intensity even though the layer was seriously distorted at high Ka. Zheng et al. [14] studied premixed H_2/air flames under various equivalence ratios in an explosion duct. Under certain ignition positions, typical tulip flames could be formed under fuel lean and fuel ultra-rich conditions, while no tulip flames could be formed under slightly rich conditions. Song et al. [15] investigated flame propagation characteristics of hydrogen enriched natural gas with φ = 0.8 - 1.2. Maximum flame speed was observed under stoichiometric condition and the speed decreases in leaner and richer flames. Under lean conditions, the flame becomes unstable due to the decreased Markstein length.

Due to the difficulty of performing fundamental studies under both high turbulent intensities and high pressures, most of high-Ka experiments are performed at atmospheric pressure or slightly elevated pressures [16-18]. The experimental system for high Ka and high pressure is usually expensive and complicated. Recently, the development of supercomputing enables three-dimensional (3D) direct numerical simulation (DNS) of turbulent flames with detailed chemistry, which helps to obtain detailed flame information that is expensive and difficult to get through experiments. DNS solves the full Navier-stokes equations, resolves turbulence from the integral length scale to Kolmogorov length scale, and could also reveal the local heat release from different chemical pathways. Wang and Luo et al. [19, 20] applied DNS to investigate hydrogen/air premixed flames with equivalence ratio 0.6 and 1.0 at moderate Ka. Due to the effects of differential diffusion, flames under lean conditions burn more vigorously in convex regions toward the unburned gas compared with the stoichiometric flames. The flame becomes diffusive-thermally unstable when combustion happens under lean conditions. Aspden et al. [21-23] conducted a series of DNS cases at moderate and high Ka under ultra-lean conditions φ = 0.31 and 0.4. It is found that the area of intense reaction in flow direction is decreased when the initial equivalence ratio increases from 0.31 to 0.4. With

increasing turbulence intensity, the density gradient across the reaction zone at φ = 0.4 decreases, which is opposite to the trend at φ = 0.31.

The aforementioned studies have provided valuable information about the heat release characteristics of premixed flames at high Ka under various lean conditions. However, most of the reported experimental and numerical studies in literature are typically at atmospheric pressure which is far below the operation condition of gas turbines. At elevated pressures, the flame thickness and speed are dramatically changed, which will modify the flame-turbulence interaction significantly. Dinesh et al. [24, 25] applied 3D DNS to premixed spherical flames at 4 atm with various equivalence ratios. They found that the flame front curvature shows a positive correlation with heat release rate under lean conditions. However, this study is performed in the thin reaction zone with moderate Ka. Wang et al. [4, 26, 27] extended DNS to turbulent combustion at 20 bar with equivalence ratios in the range of 0.39-0.5. Some cases were performed with high turbulence intensity which is relevant to lean-burn natural gas engines. However, these researches focus on flame speed and flame front structures instead of heat release characteristics. The response of heat release to equivalence ratios in high-Ka flames under high pressures is yet to be clarified.

In the present study, DNS of lean premixed H_2/air flames with detailed chemistry is performed under conditions relevant to stationary gas turbines [2]. The focus of this paper will be on the characteristics of heat release and reaction zones with various equivalence ratios. The initial Ka number is around 2335 and the pressure is 20 atm. The paper is organized as follows. Numerical methods and computational parameters are introduced in Section 2. In Section 3, the local and overall heat release characteristics of flames under different equivalence ratios are discussed. Moreover, the kinetic parameters and radical fractions of major elementary reactions are presented. In the final section, conclusions of this work are given.

2. Numerical approach

2.1. Direct numerical simulation

The simulations presented in this work are carried out using the DNS code PENCIL [28]. The compressible Navier-Stokes equations coupled with detailed transport properties and chemical kinetics are solved using a six-order explicit finite difference scheme. To reduce computational cost, mixture-averaged species transport model is adopted for species diffusion in this study, ignoring Soret and buoyancy effects. Aspden et al. [21, 22] illustrated that the mixture-averaged transport model could retain much of the qualitative behavior of lean H_2/air flames at high Ka. Preliminary analysis of laminar flames (not shown here for the sake of brevity) also indicates that the effects of equivalence ratio are qualitatively obtained even if the Soret diffusion is neglected. Moreover, it is demonstrated that the influence of buoyance is significantly reduced in flames with high turbulence intensity, especially for flames in small scales [29-31].Low-storage third-order Runge-Kutta (RK3-2N) scheme is used for time advancement and Livermore Solver for Ordinary Differential Equations (LSODE) is adopted for chemistry calculation.

The adopted chemical mechanism of H_2/O_2 was developed by Li et al. [32], which is widely used in the study of H_2 oxidation under various conditions [33-36]. Ströhle and Myhrvold [37] evaluated several detailed H_2/O_2 reaction mechanisms under gas turbine conditions, and they found that Li's mechanism shows the best agreement with experimental data in the investigation of both ignition laminar flame speed and delay time. This mechanism contains 21 reversible reactions and 9 species. In the present study, the species reaction rate is given by [38, 39]:

$$\dot{\omega} = \sum_{j=1}^{M} \left(K_f \prod_{k=1}^{N} [X_k]^{\nu'_{kj}} - K_r \prod_{k=1}^{N} [X_k]^{\nu''_{kj}} \right) \tag{1}$$

where K_f and K_r are forward and reverse reaction rate constants for reaction j. ν'_{kj} and ν''_{kj} are forward and reverse stoichiometric coefficients for species k in reaction j. X_k is the molar concentration of species k. Basically, the K_f is expressed as:

$$K_f = A_i T^{\beta_i} \exp(-E_i / R_c T) \tag{2}$$

where A_i, β_i, E_i, R_c and T are the pre-exponential factor, temperature exponent, activation energy, gas constant and temperature respectively.

In some dissociation or recombination reactions, a 'third body' is usually required. In this case, a new factor [*M*] is introduced to Equation 1 to determine the reaction rate:

$$\dot{\omega} = \sum_{j=1}^{M}[M]\left(K_f \prod_{k=1}^{N}\left[X_k\right]^{\nu'_{kj}} - K_r \prod_{k=1}^{N}\left[X_k\right]^{\nu''_{kj}} \right) \tag{3}$$

where [*M*] represents the overall contribution of different species as third bodies. In this study, the values of $[M]\bullet K_f$ and $[M]\bullet K_r$ are regarded as forward and reverse reaction rate constants for three-body reactions.

For the pressure-dependent reactions in the used mechanism, the forward rate constant is determined by:

$$K_{fh} = \left(\frac{K_0[M]}{K_\infty + K_0[M]} \right) F \tag{4}$$

where K_0 and K_∞ are the limits of low-pressure and high-pressure rate constants, which are calculated by Equation 2. In this study, the TROE approach [40, 41] is adopted to determine the factor *F*, which is more realistic and compact enough in analysing large reaction systems.

For the reversible reactions, the rate constant is given by:

$$K_r = K_f / K_{ci} \tag{5}$$

where K_{ci} is the equilibrium constant which is determined from thermodynamic properties in this study.

The chemistry implementation was validated quantitatively with Chemkin [39]. The sample applications of PENCIL code in premixed turbulent combustion could be found in [7, 28, 31, 42, 43].

2.2. Simulation parameters

Three simulations are performed in configurations with an aspect ratio of 2:1:1 as shown in Fig. 1. In order to initialise the domain, isotropic turbulence with fluctuation u' is pre-generated using helical forcing functions[44]. In addition, laminar flames are also desired to initialise the chemistry of turbulent flames. Periodic boundary conditions are applied in lateral directions, and non-reflecting Navier-Stokes Characteristics Boundary Conditions (NSCBC) [45] are applied at the inlet/outlet to

maintain the high pressure. The domain width is set to be 10 times of the integral length scale, which is higher than that of reported simulations with similar configurations [4, 42, 43, 46]. The parameters of DNS database are listed in Table 1. For all the three cases, the initial pressure is 20 atm, which is relevant to stationary gas turbines. The temperature of unburnt gas is T_u = 298 K and the equivalence ratio varies from 0.4, 0.5 to 0.6. The turbulent Reynolds number (Re) and Karlovitz number (Ka) [47] are defined as:

$$\mathrm{Re} = u' l_t / \nu \tag{6}$$

$$\mathrm{Ka} = \left(u'^3 / \nu l_t\right)^{1/2} \Big/ \left(S_L / \delta_L\right) \tag{7}$$

where u' is the root-mean-square turbulent velocity fluctuation, l_t the integral length scale, ν the kinematic viscosity, S_L the laminar flame speed and δ_L the laminar flame thickness. The flame thickness is defined by $\delta_L = (T_b - T_u) / \left|\nabla T\right|_{\max}$, where T_b and T are the burnt gas temperature and local temperature, respectively.

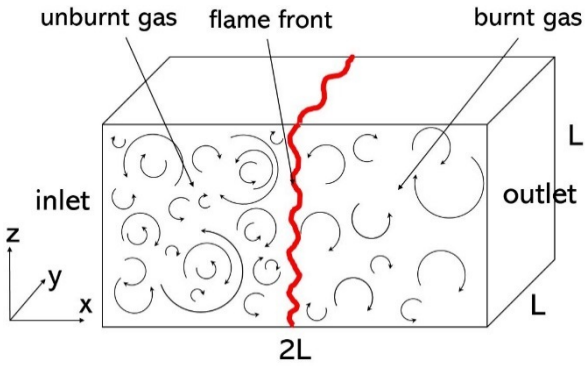

Fig. 1 - Schematic of the simulation domain.

In order to study the effects of equivalence ratio independently, the Karlovitz number and l_t/δ_L are fixed for the three simulations at different equivalence ratios. However, the Reynolds number is higher when the equivalence ratio is increased. To save computational resources, the ratio l_t/δ_L, is kept unity, which is also used in other DNS studies [48-50]. Figure 2 shows that the three cases are located in the distributed reaction zone with high u'/S_L ratio, which is more relevant to combustion in real combustors. With the increasing equivalence ratio, the laminar flame speed is increasing while the laminar flame thickness is decreasing. Correspondingly, the turbulent velocity fluctuation increases dramatically.

Table 1- Simulation parameters.

Case	A	B	C
Equivalence ratio (φ)	0.4	0.5	0.6
Laminar flame speed (S_L) (cm/s)	1.66	6.81	21.16
Laminar flame thickness (δ_L) (cm)	2.54E-02	8.3E-03	3.3E-03
Root-mean-square turbulent velocity fluctuation (u') (cm/s)	177	664	1941
Kinematic viscosity (v) (cm^2/s)	9.05E-03	9.34E-03	9.62E-03
Integral length scale (l_t) (cm)	2.54E-02	8.3E-03	3.3E-03
Grid resolution (Δx) (μm)	4.96	3.24	1.29
Turbulent Reynolds number (Re)	497	590	666
Karlovitz number (Ka)	2376	2373	2368

The domain length is 20 times the corresponding integral length scale. The domain is then discretised by uniform grids of 1024 × 512 × 512 for case A and 512 × 256 × 256 for cases B and C. As a result, the grid resolution decreases from 4.96 to 1.29 μm. To resolve the chemical scales, there are over 26 grid points across the flame thickness, which was also used for the high Ka flames in Ref. [21]. The time step is controlled by the Courant-Friedrichs-Lewy condition for computational stability. As in our previous work [7, 31], before we run the three-dimensional simulations, grid-independent tests were also carried out in two-dimensional domains to make sure the mesh used here can produce grid-independent results. The analysis is done at the time corresponding to 2 eddy turn-over time $t = 2\tau_l$ ($\tau_l = l_t / u'$) for the three cases. Carlsson et al. [46, 51] studied H_2/air flames under high Ka. They found that the flames develop rapidly in the turbulence, and a fully evolved turbulent flame could be obtained within $0.2 < t / \tau_l < 0.4$. It was demonstrated by Rutland et al. [52] that the time is slightly longer than one eddy turnover time for numerical simulation of turbulent premixed flames to achieve equilibrium status. As in our previous work [7], it was found that the mean and statistical values show monotonic variation with time after $t / \tau_l = 2$. The key information of flame front structures and chemical pathways could be qualitatively captured at $t = 2\tau_l$.

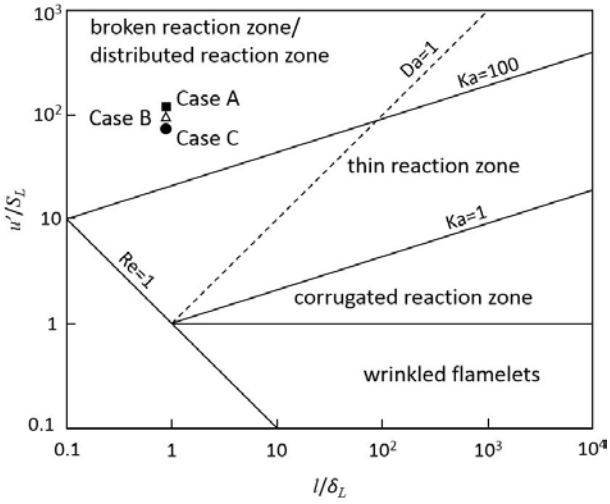

Fig. 2 - Turbulent combustion regime diagram with locations of current simulation cases.

3. Results and discussion

3.1. Overview of laminar and turbulent flames

As the turbulent flames are initialized with laminar flames, we firstly discuss the flame characteristics of laminar flames before we explore the turbulent flames. Figure 3 shows the temperature and heat release rate (HRR) profiles of laminar flames at equivalence ratio 0.4, 0.5 and 0.6, where the abscissa values are scaled by the corresponding laminar flame thickness. Table 2 lists the key parameters of the reaction zones. As expected, the burnt gas temperature increases from 1530 K to 1836 K and the HRR is dramatically enhanced when the equivalence ratio increases from 0.4 to 0.6. Correspondingly, the scaled temperature gradient in Fig. 3 is larger under higher equivalence ratio to ensure the same scaled thermal thickness δ_L. However, it should be noted that the reaction zone is thinner than thermal thickness in the studied cases. Hereby, the reaction zone is defined as regions with heat release rate higher than 10% threshold of corresponding laminar flames. When the equivalence ratio increases, the reaction zone is obviously broadened. As shown in Table 2, the reaction layer thickness of laminar flames increases from 0.54 δ_L to δ_L when the equivalence ratio increases from 0.4 to 0.6. Moreover, two characteristic temperatures of laminar flames are presented. The temperature corresponding to maximum temperature gradient fluctuates around 1200 K; the temperature corresponding to peak heat release rate increases with increasing equivalence ratio, from 1403 K to 1543 K.

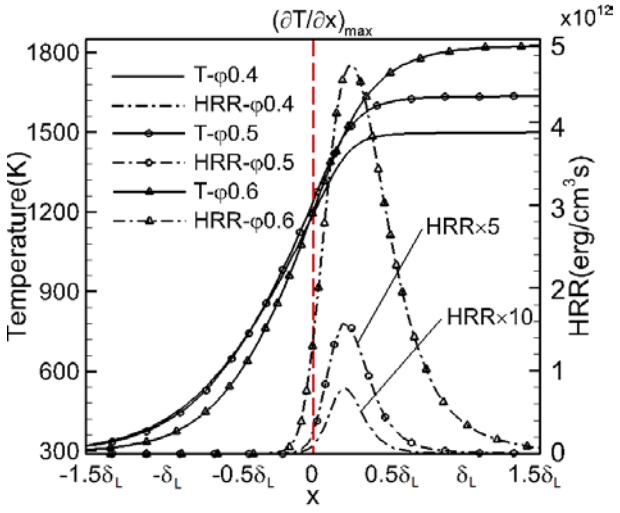

Fig. 3 - Structures of lean premixed laminar flames at different equivalence ratios. The red dashed line denotes the abscissa value which corresponds to the maximum temperature gradient.

Next, the reaction zone characteristics of turbulent flames with φ = 0.4, 0.5 and 0.6 are discussed. Figure 4 presents the reaction layer structures coloured by temperature and Fig. 5 shows the mean heat release rate versus progress variable which is defined as:

$$c = \left(Y_{u,H_2} - Y_{f,H_2}\right) / \left(Y_{u,H_2} - Y_{b,H_2}\right) \tag{8}$$

where Y_{u,H_2} is the H_2 mass fraction in the fresh mixture, Y_{f,H_2} is the local H_2 mass fraction and Y_{b,H_2} is the H_2 mass fraction in the burnt gas.

Table 2 - Characteristic parameters of reaction zones of laminar and turbulent flames

Case	HRR_{max_1D} (erg/cm^{3}s)	Mean HRR_{max_3D} (erg/cm^{3}s)	δ_{f_1D}	δ_{f_3D}	T_1 (K)	T_2 (K)
A	7.90E10	3.69E11	0.54 δ_L	1.25 δ_L	1188	1403
B	7.87E11	1.95E12	0.65 δ_L	1.63 δ_L	1238	1478
C	4.68E12	6.73E12	δ_L	1.86 δ_L	1196	1543

δ_f - reaction layer thickness

Mean HRR_{max_3D} - maximum conditional mean of HRR on progress variable in turbulent flames

T_1 - temperature corresponds to maximum temperature gradient of laminar flames

T_2 - temperature corresponds to peak heat release rate of laminar flames

Table 2 also gives the key parameters of turbulent flames. The average reaction layer thickness of turbulent flame is defined as $\delta_f = V_{rec} / S_{yz}$, where the reaction zone volume V_{rec} is the volume of regions with heat release higher than 10% threshold of the corresponding laminar flames and the cross-section area $S_{yz} = L^2$ is the area of *y*-*z* slice across the domain as shown in Fig. 1. For laminar flames, the reaction layer thickness is determined directly from the profile of heat release rate versus flame position *x*. Since the three cases are characterized by the same Ka, the flame fronts show analogous structures in Fig. 4. Similar to the laminar flames, the heat release of turbulent flames is enhanced, and the reaction layer is relatively broadened under high equivalence ratio. Correspondingly, the reaction zone covers a wider range of temperature at high φ. These differences under various equivalence ratios are attributed to the differential diffusion effect in premixed combustion [20]. In Fig. 5, obvious heat release is observed from c = 0.4 for case φ = 0.6 while it happens after c = 0.7 for case φ = 0.4. It is also noted that the reaction layers of turbulent flames are thicker than the corresponding thermal thicknesses, and the thickness increases with increasing equivalence ratio. Although the turbulent flames exhibit similar trends to laminar flames with varying equivalence ratios, the extent of enhancement is reduced at high equivalence ratio. For example, the peak conditional mean of heat release rate for the turbulent flame with φ = 0.4 is 3.7 times higher than that of the corresponding laminar flame, while the value is only 0.4 times higher for the turbulent flame with φ = 0.6. The reaction layer thickness almost doubles in the laminar flames when the equivalence ratio increases from 0.4 to 0.6. For the turbulent flames, the thickness only increases from 1.25 δ_L to 1.86 δ_L. One possible explanation is that the enhanced heat release of turbulent H_2/air flame is a combined result of turbulent transport and species diffusion, but the turbulent transport is overtaking differential diffusion as the main effect when the flame transitions to the distributed reaction mode.

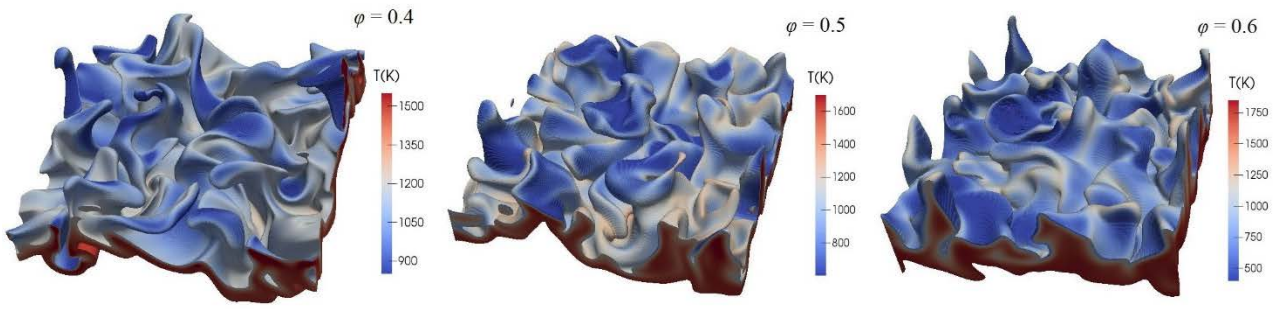

Fig. 4 - Reaction zone structures of lean premixed turbulent flames at different equivalence ratios.

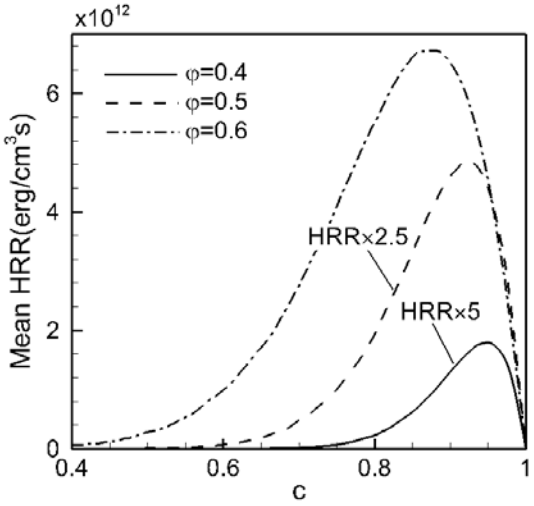

Fig. 5 - Conditional mean of heat release rate on progress variable for turbulent flames at different equivalence ratios.

3.2. Characteristics of turbulent reaction zones

In this section, we discuss the local and statistical values regarding the heat release in turbulent reaction zones. Figure 6 shows the zoomed-in contours of local equivalence ratio in the flame brush, where the reaction layers are bounded by the white solid lines and the local φ plateaus ($\varphi_L > 1.1\ \varphi$) are bounded by the solid black lines. The local equivalence ratio φ_L is defined as:

$$\varphi_L = \frac{Y_H/(2\cdot W_H)}{Y_O/W_O} \tag{9}$$

where Y_H and Y_O are mass fractions of hydrogen and oxygen element, and W_H and W_O are molar mass of hydrogen and oxygen element, respectively. The contours indicate the presence of differential diffusion in the studied cases. It is obviously noted that φ_L is significantly lower than the fresh gas φ in the upstream near the reaction layer and all the φ_L plateaus of the three cases locate in the reaction

layer. Hereby, we define the left boundary of the reaction zone as 'φ_L cliff', the convex region towards the unburned side is characterised by positive curvature and the concave region is characterised by negative curvature. It is interesting to find that the φ_L trenches and plateaus are situated on both sides of the cliff, which is much like the natural topography. The temperature gradient near φ_L cliff is observed to be high at positive curvatures, and low at negative curvatures. However, the difference in temperature gradient between positive and negative curvatures is reduced with increasing φ. Furthermore, the trench 'depth' and plateau 'height' are reduced as the φ is increased. This is primarily due to the decrease of the Lewis number with increasing φ, which promotes a diffusive-thermally stable flame [19].

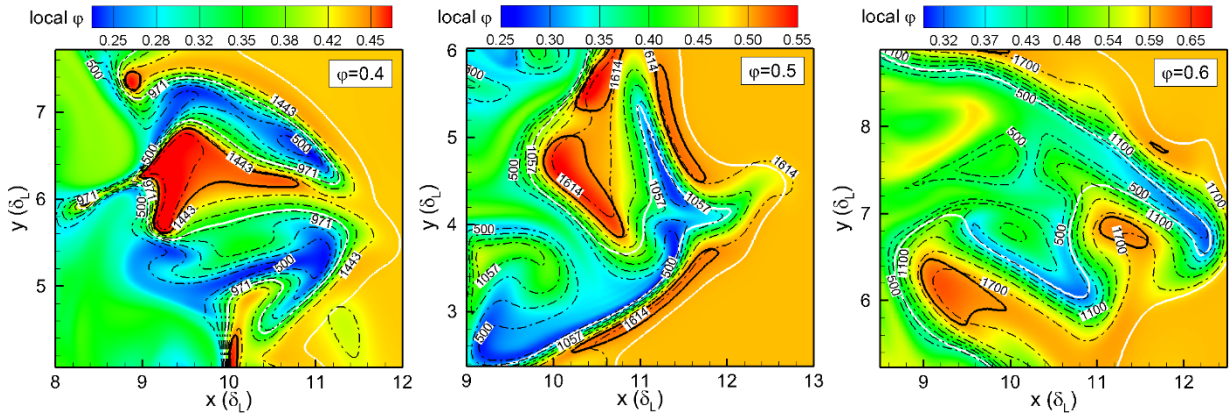

Fig. 6 - Two-dimensional slices of the reaction zone coloured by local equivalence ratio. The black dashed lines correspond to temperature levels, the solid black lines bound the local φ plateaus and the white solid lines bound the reaction zone.

Since the φ_L cliff area is also characterized by a high gradient of temperature in Fig. 6, it is necessary to shed more light on the correlation of temperature, φ_L and heat release rate. Figure 7 shows the scattered φ_L versus temperature in the reaction zone, where the scatters are coloured by local heat release rate. The adiabatic temperature of the corresponding laminar flame is also indicated in the plots. Overall, the scatter distribution shows a positive correlation between φ_L and temperature for the three cases. Nevertheless, the broader scatter distribution of Case φ = 0.6 indicates that the correlation rate is reduced when φ is increased. It is interesting to note that there are many hot spots above the adiabatic temperature under leaner conditions. For example, for Case φ = 0.4, the adiabatic

laminar flame temperature is 1530 K, while the peak temperature of the turbulent flame exceeds 1800 K. On the other hand, the temperature of the whole reaction zone is below the adiabatic temperature for Case φ = 0.6. A similar trend was also reported by Aspden et al. [21] for lean premixed H_2/air flames under atmospheric pressure. In their study, hot spots appear under ultra-lean condition (φ = 0.31) despite Ka. At φ = 0.4, hot spots are observed at low to moderate Ka, while they disappear in distributed flames. In the current study, hot spots still exist in the high-Ka flames at φ = 0.4 and 0.5, which is mainly attributed to the pressure effects on reaction zone structures. As mentioned before, lean-premixed combustion has the potential to reduce NO_x emission due to low peak combustion temperature. However, temperature in the hot regions under ultra-lean conditions (Case φ = 0.4) would exceed the adiabatic temperature to a large extent, which will contribute to the formation of NO_x. This result is instructive and meaningful for industrial application of lean-premixed combustion.

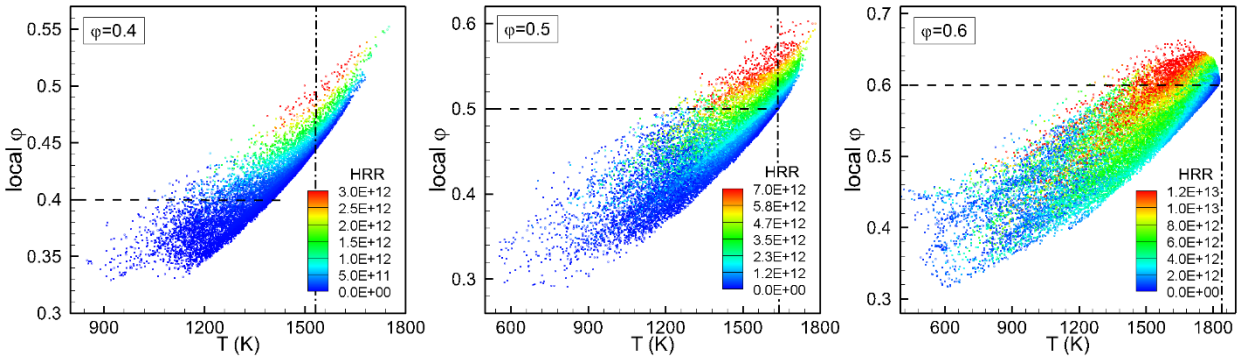

Fig. 7 - Scatter plots of local temperature and local equivalence ratio in the reaction zone. The scatters are coloured by local heat release rate. The horizontal dashed lines denote the equivalence ratio in the unburned gas and the vertical dashed lines denote the peak temperatures of the corresponding laminar flames.

The presence of hot spots is a consequence of extended φ_L above unburnt mixture φ under leaner condition. As indicated in Fig. 7, the φ_L extends to about 0.15 higher than the mixture φ for Case φ = 0.4, while the value is only around 0.05 for Case φ = 0.6. As the Lewis number is decreasing with increasing equivalence ratio, the diffusion of light species (e.g. H_2, H) will be enhanced at φ = 0.6 and the reaction zone will be broadened as seen on Table 2. As a result, the species distribution and heat release are more uniform in the reaction zone. By contrast, the heat release is more intense in

the narrow reaction zone and hot spots appear at φ = 0.4. Furthermore, the heat release rate shows a positive correlation with both temperature and φ_L. However, the HRR gradient is decreasing across temperature with increasing φ. For example, the tail of Case φ = 0.6 in Fig. 7 is coloured by blue and green (low and moderate HRR), while the tail of Case φ = 0.4 is only coloured by blue (low HRR). This observation agrees with the results shown in Fig. 6. For high-Ka flames at atmospheric pressure, turbulence transport is becoming dominate and the effects of differential diffusion is diminishing [51, 53].However, the profiles of local equivalence ratio in Fig. 7 illustrate that differential diffusion is still significant in the current high-Ka cases at 20 atm, which is attributed to the thinner reaction regions at high pressures.

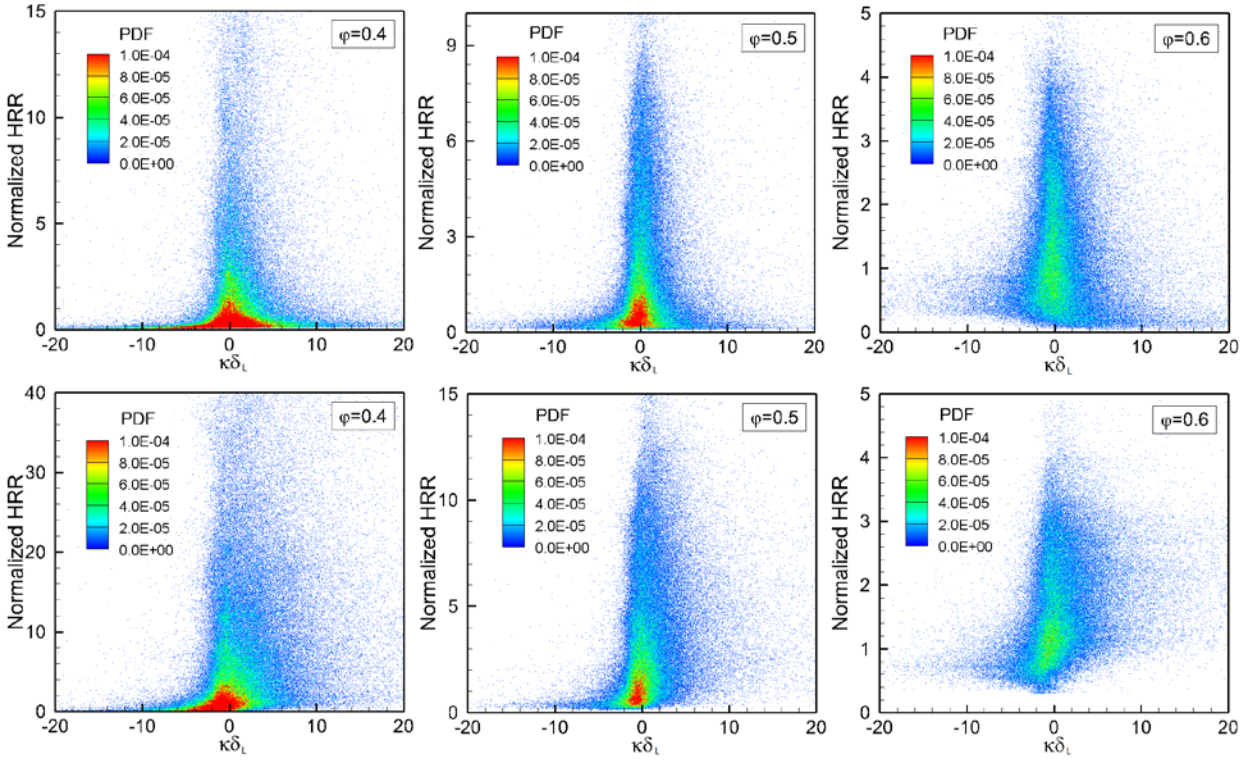

Fig. 8 - Scatter plots of curvature and normalised heat release rate on the iso-surfaces with corresponding temperature T_1 (top row) and T_2 (bottom row) as indicated in Table 2. The curvature is scaled by the corresponding laminar flame thickness.

To shed more light on the effects of flame structures on the heat release rate, two temperature iso-surfaces in the reaction zone are selected, and the probability density function (PDF) for scaled curvature and normalised HRR is shown in Fig. 8. The two temperatures, T_1 and T_2 as indicated in

Table 2, respectively, correspond to maximum temperature gradient and peak heat release rate in laminar flames. The mean curvature is defined as $\kappa = -\nabla \bullet \hat{n}$, where $\hat{n} = -\nabla T / |\nabla T|$ is the unit normal vector of the flame front. In Fig. 8, the mean curvature is scaled by the corresponding laminar flame thickness and the value is positive for the convex regions towards the unburned side. For iso-surfaces of T_1, the scatters show a normal distribution for Case φ = 0.4 and 0.5, although the HRR of positive curvatures is relatively higher than that of negative curvatures. Nevertheless, the behaviour of the heat release rate distribution for Case φ = 0.6 differs from the other two cases. The lowest HRR occurring in positive curvature regions is higher than that in negative curvature regions. It should be noted that the PDF gradient is decreasing with increasing equivalence ratio, which means the enhancement (weakening) of reaction rate in convex (concave) regions is reducing as equivalence ratio is increased. This finding is consistent with the results of Luo et al. [20] for H_2/air flames under lean and stoichiometric conditions at the atmospheric pressure. Dinesh et al. [25] also observed weak burning structures in concave regions under lean conditions in spherical flames under elevated pressures.

On iso-surfaces of T_2, the aforementioned trends still exist and become more obvious. The HRR in convex regions is significantly enhanced even for Case φ = 0.6. Moreover, the peak HRR happens in low curvature regions, which is due to the effects of the Markstein number [48]. Comparing the ordinate values of the two set plots, it is found that the gap is decreasing with increasing equivalence ratio. For example, the ordinate threshold increases from 15 to 40 as the temperature increases from T_1 to T_2 at φ = 0.4, while the threshold reaches the same value 5 at φ = 0.6. It indicates that the heat release gradient is specially reduced under high equivalence ratio. Overall, the response of HRR to local curvature is changing with equivalence ratio and either set of the iso-surfaces can present the trend of change.

In Fig. 6, the isoline of T_1 is very close to the left boundary of the reaction layer. Thus, flame front structures are statistically identified by the T_1 iso-surface for the three cases. Figure 9 presents the probability density functions (PDFs) of flame front curvatures. The mean curvatures are scaled

by the thickness of corresponding laminar flames. The statistical result shows that the flame front structures are quite similar in the three flames, despite the peak value for flame φ = 0.5 is a little bit smaller. Similar distribution is also observed by Wang et al. [4] in lean premixed methane/air flames with φ = 0.39 – 0.5 under low Ka. It indicates that the variation of equivalence ratio can not change flame front wrinkling in both thin reaction zone and distributed reaction zone when Ka is fixed.

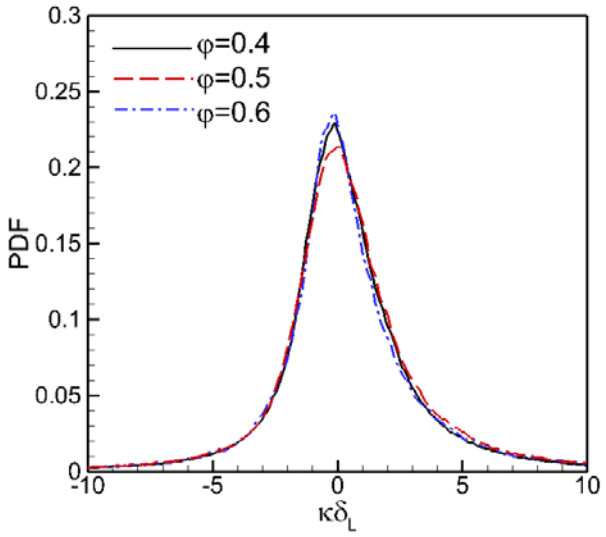

Fig. 9 - PDFs of mean curvatures of flame fronts for cases under different equivalence ratios. The mean curvatures are scaled by corresponding laminar flame thicknesses.

3.3. The response of elementary reactions to equivalence ratio variation

As a multi-step chemical mechanism is adopted in this study, the heat release we mentioned above is the overall presentation of all the elementary reactions. When the equivalence ratio varies, the radical distribution and elementary reaction must be affected. Studying the heat release from main elementary reactions will extend our understanding of premixed flames. There are 21 reversible reactions in the used mechanism and the five elementary reactions listed in Table 3 contribute to ~90% of the total heat releases.

Table 3 Main reactions of Li et al. H_2/O_2 mechanism

#	Reaction	#	Reaction
Reaction3 (R3)	$H_2 + OH = H_2O + H$	Reaction8 (R8)	$H + OH + M = H_2O + M$
Reaction9 (R9)	$H + O_2 (+M) = HO_2 (+M)$	Reaction11 (R11)	$HO_2 + H = OH + OH$

Reaction13 (R13) $HO_2 + OH = H_2O + O_2$

Firstly, Figure 10 presents the average heat release rate of the selected 5 elementary reactions versus temperature in the reaction zones of turbulent flames at different equivalence ratios. As expected, the elementary reactions show high HRR above the adiabatic temperature in Case φ = 0.4 and 0.5, which will contribute to the hot spots in the reaction zones. Before reaching the adiabatic temperature, every reaction exhibits a HRR peak. It is noticed that the HRR peak arises from 1200 K for all the three cases, while the slope is decreasing with increasing equivalence ratio. Moreover, the heat release under moderate temperatures (600-1200 K) is significantly enhanced when the equivalence ratio is increased from 0.4 to 0.6, especially for the dominating reactions R9 and R13. In the high-temperature regions (T > 1200 K), the heat release contributions from R3 and R8 are more prominent with increasing equivalence ratios. R3 overtakes R13 as the second most dominating reaction in Case φ = 0.6.

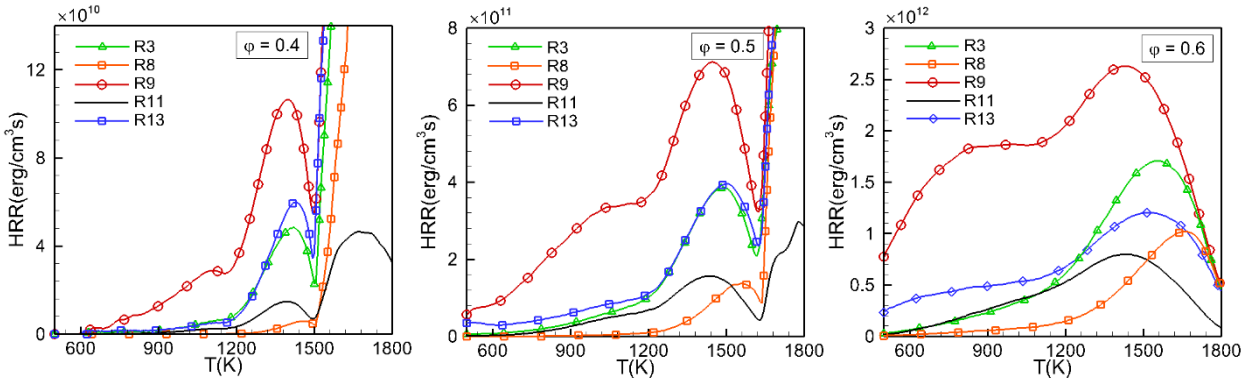

Fig. 10 – Conditional mean of heat release rate on temperature for elementary reactions in turbulent flames.

As shown in Eqs. 1 and 3, two key factors, rate constant K and species concentration X_k, directly determine the reaction rate. Thus, the species concentrations and rate constants as a function of temperature are presented in Figs. 11 and 12 to assist the discussion of heat release in reaction zones. Overall, it is seen in Fig. 11 that the fractions of all species are obviously increased with increasing equivalence ratio, which can explain the enhanced heat release rate under high φ. When the temperature is higher than adiabatic temperature, it is noted that there exist considerable radicals for Case φ = 0.4 and 0.5, which will lead to the formation of hot spots in the reaction zone. This

observation is consistent with the φ_L plateaus in Fig. 6. Although differential diffusion is expected to be less important under high Ka [21], the effects are still considerable when the equivalence ratio is increased in this study. From Fig. 11, it is evident that the diffusion of H and OH is enhanced under high φ, leading to a broader and uniform distribution.

In Fig. 12, it is seen that the rate constants of reverse reactions are negligible compared with that of forward reactions, despite the relatively high rate constant of reverse reaction R3 under high temperature. So, in the following discussion of elementary reactions, we only consider the positive reactions. For R9 and R13, the positive reaction rates show exponential decay with increasing temperature. On the other hand, the mole fractions of H and OH are increased in moderate-temperature regions for Case φ = 0.6. As a result, the heat release is enhanced in moderate temperatures for Case φ = 0.6 in Fig. 10. For reaction 3, the positive reaction rate and OH mole fraction all experience exponential growth with increasing temperature, which is more significant under higher equivalence ratio. These dual effects promote the reaction of R3 under high φ, which explains why R3 overtakes R13 as the second most dominating reaction for Case φ = 0.6. It is also noted in Fig. 10 that R8 is enhanced in high-temperature regions under high φ. This could possibly be attributed to the high contribution of H_2O to third-body [M] in Eq. 3. When the equivalence ratio is increased, the H_2O concentration under high temperatures is also increased, which will contribute to a high [M] value. For R11, the positive rate constant levels off after 1000 K. Thus, although the HRR of R11 is increased, the difference between moderate-temperature and high-temperature regions is not as evident as other reactions.

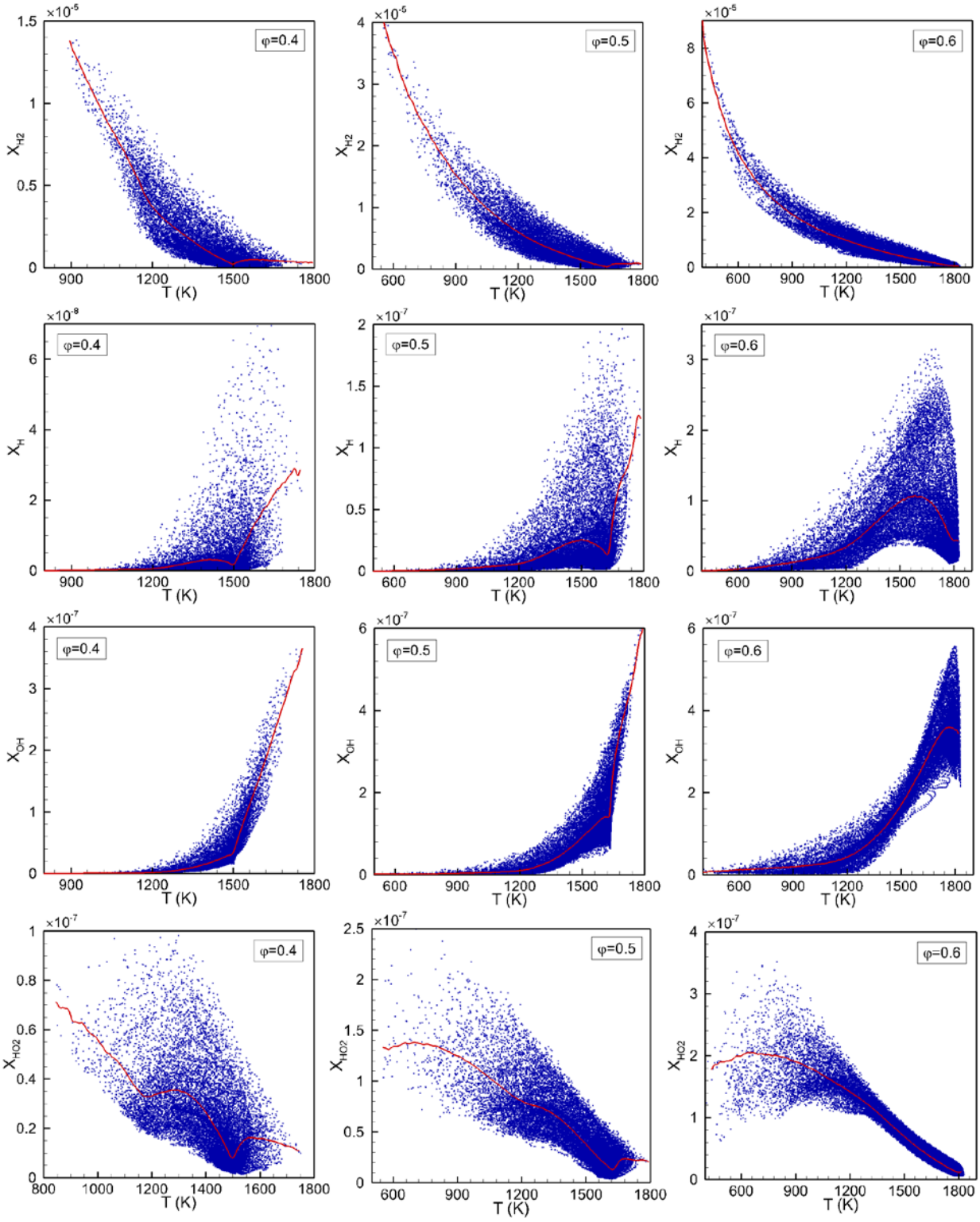

Fig. 11 - Scatter plots of main species mole fractions in the reaction zone. The solid red lines denote the mean values conditioned on temperature.

1

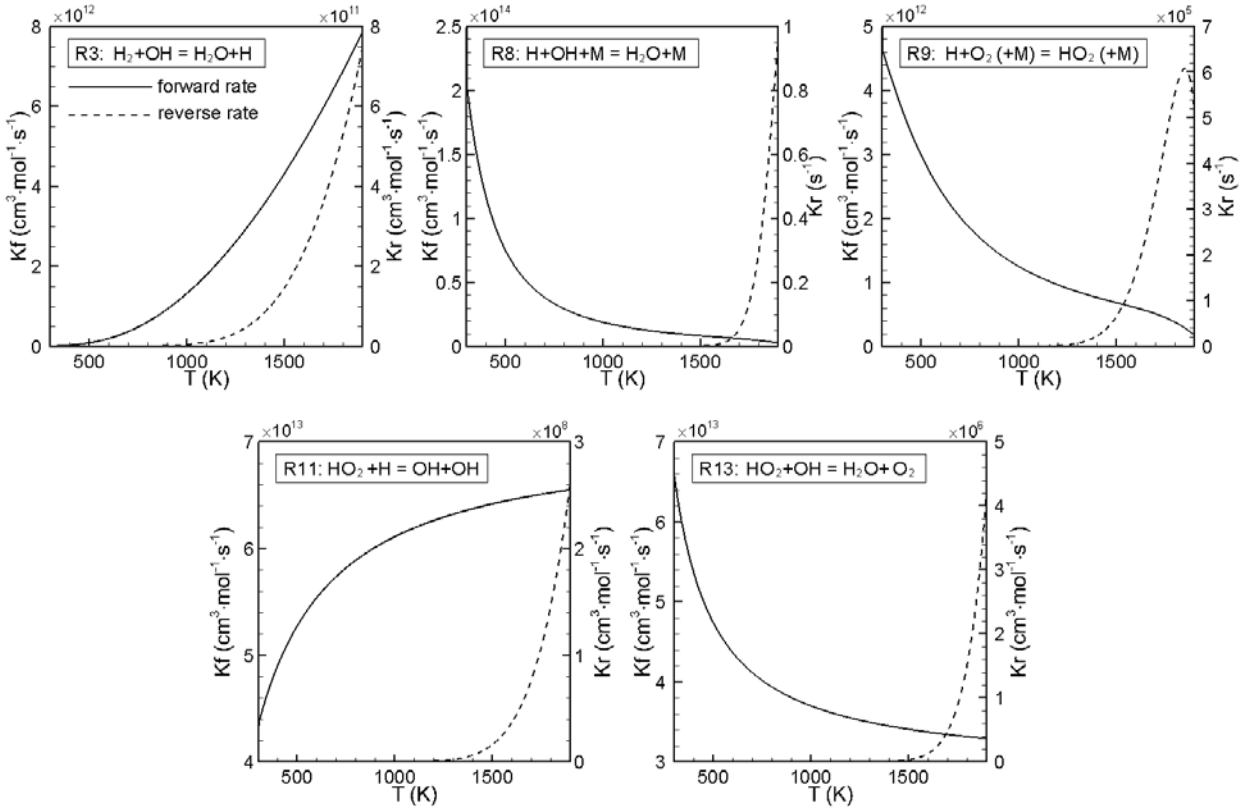

Fig. 12 - Forward and reverse reaction rate constants versus temperature for the main heat release reactions. The solid lines denote the forward reaction rate and the dashed lines denote the reverse reaction rate.

4. Conclusions

In this study, three-dimensional direct numerical simulations of H_2/air flames are carried out to investigate the characteristics of heat release under various equivalence ratios. These flames are simulated at high Karlovitz number and high pressures which are relevant to lean-burn gas turbine conditions. Reaction zone structures, local equivalence ratio, flame front curvature and elementary reaction rates are examined statistically with the objective of extending our understanding of lean combustion under high-pressure conditions.

Under different lean conditions (φ = 0.4, 0.5, 0.6), the turbulent flame fronts show similar topological structures for the three cases under the same Karlovitz number, even though the higher φ case is characterized with stronger heat release rate. It is also noted that the relative thickness of reaction zone (δ_f / δ_L) is increasing for both laminar and turbulent flames with increasing equivalence ratio. However, the extent of increase for heat release and reaction layer thickness is reduced under

high φ, which indicates that turbulent transport is overtaking differential diffusion as the main effect on the high Ka flames.

The turbulent flames behave differently in positive and negative curvature regions. It is observed that the trenches of local equivalence ratio φ_L are located at concave structures inside the reaction zone, while φ_L plateaus are situated at convex structures outside the reaction zone. With increasing equivalence ratio, the trench 'depth' and plateau 'height' are reduced, which is primarily due to the decreased Lewis number. In addition, φ_L is found to be significantly higher than mixture φ under ultra-lean conditions, resulting in hot spots in the reaction zone. This finding suggests that the benefits of lean combustion in terms of lowering peak flame temperature and reducing NOx emission may be slightly cut down under ultra-lean conditions, which is instructive for industrial applications. Furthermore, the temperature iso-surfaces show that the enhancement (weakening) of heat release in convex (concave) regions is reduced as φ is increased in the reaction zone.

The heat release behaviour in the reaction zone is explained by analysing radical distribution and rate constant as a function of temperature. At high equivalence ratio, the radical transportation and concentration are significantly increased. The high radical fractions in regions with over-adiabatic temperature contribute to the formation of hot spots directly under ultra-lean conditions. As the rate constants of reaction $H + O_2 (+M) = HO_2 (+M)$ and $HO_2 + OH = H_2O + O_2$ decay exponentially with increasing temperature, their heat releases are relatively enhanced in moderate-temperature regions, which contributes to a broadened reaction zone for the case with higher equivalence ratio. In summary, due to the combined effects of radical fractions and reaction rate constants, the local heat release is changed in different temperature windows when the mixture equivalence ratio varies.

Acknowledgement

This work was supported by the UK Engineering and Physical Sciences Research Council under the projects "UK Consortium on Mesoscale Engineering Sciences (UKCOMES)" (Grant Nos. EP/L00030X/1 and EP/R029598/1) and "High Performance Computing Support for United Kingdom

Consortium on Turbulent Reacting Flow (UKCTRF)" (Grant No. EP/K024876/1). Sponsorships for Mr Xujiang Wang by University College London and China Scholarship Council are gratefully acknowledged. Tai Jin acknowledges the financial support by the National Natural Science Foundation of China (No. 51576176).

References

[1] Lefebvre AH, Ballal DR. Gas turbine combustion: alternative fuels and emissions: CRC press; 2010.

[2] Jansohn P. Modern gas turbine systems: High efficiency, low emission, fuel flexible power generation: Elsevier; 2013.

[3] Murat Altay H, Speth RL, Hudgins DE, Ghoniem AF. The impact of equivalence ratio oscillations on combustion dynamics in a backward-facing step combustor. Combust Flame. 2009;156:2106-16.

[4] Wang Z, Motheau E, Abraham J. Effects of equivalence ratio variations on turbulent flame speed in lean methane/air mixtures under lean-burn natural gas engine operating conditions. Proc Combust Inst. 2017;36:3423-30.

[5] Strakey P, Sidwell T, Ontko J. Investigation of the effects of hydrogen addition on lean extinction in a swirl stabilized combustor. Proc Combust Inst. 2007;31:3173-80.

[6] Goswami M, van Griensven JGH, Bastiaans RJM, Konnov AA, de Goey LPH. Experimental and modeling study of the effect of elevated pressure on lean high-hydrogen syngas flames. Proc Combust Inst. 2015;35:655-62.

[7] Wang X, Jin T, Xie Y, Luo KH. Effects of pressure and Karlovitz number on the turbulence-flame interactions in lean premixed H_2/air flames. Fuel. 2018;234:1293-300.

[8] !!! INVALID CITATION !!! [8, 9].

[9] !!! INVALID CITATION !!! [4, 9, 10].

[10] Peters N. Turbulent combustion. Cambridge: Cambridge University Press; 2000.

[11] Stopper U, Meier W, Sadanandan R, Stöhr M, Aigner M, Bulat G. Experimental study of industrial gas turbine flames including quantification of pressure influence on flow field, fuel/air premixing and flame shape. Combust Flame. 2013;160:2103-18.

[12] Zhou B, Brackmann C, Li Q, Wang Z, Petersson P, Li Z, et al. Distributed reactions in highly turbulent premixed methane/air flames. Combust Flame. 2015;162:2937-53.

[13] Skiba AW, Wabel TM, Carter CD, Hammack SD, Temme JE, Driscoll JF. Premixed flames subjected to extreme levels of turbulence part I: Flame structure and a new measured regime diagram. Combust Flame. 2018;189:407-32.

[14] Zheng L, Zhu X, Wang Y, Li G, Yu S, Pei B, et al. Combined effect of ignition position and equivalence ratio on the characteristics of premixed hydrogen/air deflagrations. Int J Hydrogen Energy. 2018;43:16430-41.

[15] Song Z, Zhang X, Hou X, Li M. Effect of initial pressure, temperature and equivalence ratios on laminar combustion characteristics of hydrogen enriched natural gas. Journal of the Energy Institute. 2017.

[16] Zhou B, Brackmann C, Wang Z, Li Z, Richter M, Aldén M, et al. Thin reaction zone and distributed reaction zone regimes in turbulent premixed methane/air flames: Scalar distributions and correlations. Combust Flame. 2017;175:220-36.

[17] Sjöholm J, Rosell J, Li B, Richter M, Li Z, Bai X-S, et al. Simultaneous visualization of OH, CH, CH2O and toluene PLIF in a methane jet flame with varying degrees of turbulence. Proc Combust Inst. 2013;34:1475-82.

[18] Duwig C, Li B, Li ZS, Aldén M. High resolution imaging of flameless and distributed turbulent combustion. Combust Flame. 2012;159:306-16.

[19] Wang H, Luo K, Qiu K, Lu S, Fan J. A DNS study of hydrogen/air swirling premixed flames with different equivalence ratios. Int J Hydrogen Energy. 2012;37:5246-56.

[20] Luo K, Wang H, Bushe WK, Fan J. Direct numerical simulation and reaction rate modelling of premixed turbulent flames. Int J Hydrogen Energy. 2014;39:12158-65.

[21] Aspden AJ, Day MS, Bell JB. Turbulence-flame interactions in lean premixed hydrogen: transition to the distributed burning regime. J Fluid Mech. 2011;680:287-320.

[22] Aspden AJ, Day MS, Bell JB. Turbulence-chemistry interaction in lean premixed hydrogen combustion. Proc Combust Inst. 2015;35:1321-9.

[23] Aspden AJ. A numerical study of diffusive effects in turbulent lean premixed hydrogen flames. Proc Combust Inst. 2017;36:1997-2004.

[24] Ranga Dinesh KKJ, Shalaby H, Luo KH, van Oijen JA, Thévenin D. High hydrogen content syngas fuel burning in lean premixed spherical flames at elevated pressures: Effects of preferential diffusion. Int J Hydrogen Energy. 2016;41:18231-49.

[25] Ranga Dinesh KKJ, Shalaby H, Luo KH, van Oijen JA, Thévenin D. Heat release rate variations in high hydrogen content premixed syngas flames at elevated pressures: Effect of equivalence ratio. Int J Hydrogen Energy. 2017;42:7029-44.

[26] Wang Z, Magi V, Abraham J. Turbulent flame speed dependencies in lean methane-air mixtures under engine relevant conditions. Combust Flame. 2017;180:53-62.

[27] Wang Z, Abraham J. Effects of Karlovitz number on flame surface wrinkling in turbulent lean premixed methane-air flames. Combust Sci Technol. 2017;190:363-92.

[28] Babkovskaia N, Haugen NEL, Brandenburg A. A high-order public domain code for direct numerical simulations of turbulent combustion. J Comput Phys. 2011;230:1-12.

[29] Libby PA. Theoretical analysis of the effect of gravity on premixed turbulent flames. Combust Sci Technol. 1989;68:15-33.

[30] Cheng RK, Bédat B, Kostiuk LW. Effects of buoyancy on lean premixed V-flames Part I: laminar and turbulent flame structures. Combust Flame. 1999;116:360-75.

[31] Wang X, Jin T, Xie Y, Luo KH. Pressure effects on flame structures and chemical pathways for lean premixed turbulent H_2/air flames: Three-dimensional DNS studies. Fuel. 2018;215:320-9.

[32] Li J, Zhao Z, Kazakov A, Dryer FL. An updated comprehensive kinetic model of hydrogen combustion. Int J Chem Kinet. 2004;36:566-75.

[33] Ribert G, Zong N, Yang V, Pons L, Darabiha N, Candel S. Counterflow diffusion flames of general fluids: Oxygen/hydrogen mixtures. Combust Flame. 2008;154:319-30.

[34] Chen Z, Burke MP, Ju Y. Effects of Lewis number and ignition energy on the determination of laminar flame speed using propagating spherical flames. Proc Combust Inst. 2009;32:1253-60.

[35] Yoo CS, Sankaran R, Chen J. Three-dimensional direct numerical simulation of a turbulent lifted hydrogen jet flame in heated coflow: flame stabilization and structure. J Fluid Mech. 2009;640:453-81.

[36] Lu T, Yoo CS, Chen J, Law CK. Three-dimensional direct numerical simulation of a turbulent lifted hydrogen jet flame in heated coflow: a chemical explosive mode analysis. J Fluid Mech. 2010;652:45-64.

[37] Strohle J, Myhrvold T. An evaluation of detailed reaction mechanisms for hydrogen combustion under gas turbine conditions. Int J Hydrogen Energy. 2007;32:125-35.

[38] Poinsot T, Veynante D. Theoretical and numerical combustion. Bordeaux: RT Edwards; 2005.

[39] Kee RJ, Rupley FM, Meeks E, Miller JA. CHEMKIN-III: A FORTRAN chemical kinetics package for the analysis of gas-phase chemical and plasma kinetics. Sandia national laboratories report SAND96-8216. 1996.

[40] Troe J. Theory of thermal unimolecular reactions in the fall-off range. I. Strong collision rate constants. Berichte der Bunsengesellschaft für physikalische Chemie. 1983;87:161-9.

[41] Gilbert R, Luther K, Troe J. Theory of thermal unimolecular reactions in the fall-off range. II. Weak collision rate constants. Berichte der Bunsengesellschaft für physikalische Chemie. 1983;87:169-77.

[42] Uranakara HA, Chaudhuri S, Dave HL, Arias PG, Im HG. A flame particle tracking analysis of turbulence-chemistry interaction in hydrogen–air premixed flames. Combust Flame. 2016;163:220-40.

[43] Chaudhuri S. Life of flame particles embedded in premixed flames interacting with near isotropic turbulence. Proc Combust Inst. 2015;35:1305-12.

[44] Brandenburg A. The inverse cascade and nonlinear alpha-effect in simulations of isotropic helical hydromagnetic turbulence. Astrophys J. 2001;550:824-40.

[45] Lodato G, Domingo P, Vervisch L. Three-dimensional boundary conditions for direct and large-eddy simulation of compressible viscous flows. J Comput Phys. 2008;227:5105-43.

[46] Carlsson H, Yu R, Bai X-S. Flame structure analysis for categorization of lean premixed CH_4/air and H_2/air flames at high Karlovitz numbers: Direct numerical simulation studies. Proc Combust Inst. 2015;35:1425-32.

[47] Poinsot T, Veynante D, Candel S. Quenching processes and premixed turbulent combustion diagrams. J Fluid Mech. 1991;228:561-606.

[48] Savard B, Lapointe S, Teodorczyk A. Numerical investigation of the effect of pressure on heat release rate in iso-octane premixed turbulent flames under conditions relevant to SI engines. Proc Combust Inst. 2017;36:3543-9.

[49] Lapointe S, Savard B, Blanquart G. Differential diffusion effects, distributed burning, and local extinctions in high Karlovitz premixed flames. Combust Flame. 2015;162:3341-55.

[50] Hamlington PE, Poludnenko AY, Oran ES. Interactions between turbulence and flames in premixed reacting flows. Phys Fluids. 2011;23:125111.

[51] Carlsson H, Yu R, Bai X-S. Direct numerical simulation of lean premixed CH_4/air and H_2/air flames at high Karlovitz numbers. Int J Hydrogen Energy. 2014;39:20216-32.

[52] Rutland CJ, Ferziger JH, El Tahry SH. Full numerical simulations and modeling of turbulent premixed flames. Symposium (International) on Combustion: Elsevier; 1991. p. 621-7.

[53] Aspden AJ, Day MS, Bell JB. Lewis number effects in distributed flames. Proc Combust Inst. 2011;33:1473-80.